The effect of pre-oxidation parameters on the corrosion behavior of AISI 441 in dual atmosphere

Available online at www.sciencedirect.com

ScienceDirect

journal homepage: www.elsevier.com/locate/he

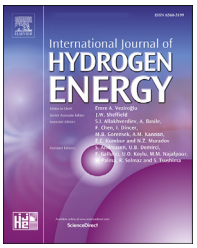

The effect of pre-oxidation parameters on the corrosion behavior of AISI 441 in dual atmosphere

Claudia Goebel[*], *Patrik Alnegren*, *Robin Faust*, *Jan-Erik Svensson*, *Jan Froitzheim*

Chalmers University of Technology, Department of Chemistry and Chemical Engineering, Division of Energy and Materials, Kemivägen 10, 41296 Gothenburg, Sweden

ARTICLE INFO

Article history:
Received 17 April 2018
Received in revised form
24 May 2018
Accepted 30 May 2018
Available online 23 June 2018

Keywords:
Solid oxide fuel cell
Interconnect
Corrosion
Dual atmosphere
Pre-oxidation

ABSTRACT

Dual atmosphere conditions have been shown to be detrimental for the ferritic stainless steel interconnects used in solid oxide fuel cells (SOFC) under certain conditions. In the present work, we analyze the influence of pre-oxidation on corrosion resistance in dual atmosphere with regard to two parameters: the pre-oxidation time and the pre-oxidation location (pre-oxidation layer on the air-facing side or the hydrogen-facing side). The steel AISI 441 is investigated and pre-oxidation is achieved in air at 800 °C. To examine the influence of pre-oxidation time on corrosion behavior, five different pre-oxidation times are used: 0, 11, 45, 180, and 280 min. The samples are exposed discontinuously to dual atmosphere for 1000 h at 600 °C. Photographs, taken throughout the exposure, show that the pre-oxidation time correlates with the onset of breakaway corrosion. To analyze the influence of pre-oxidation location on corrosion behavior, the samples are pre-oxidized for 180 min, and then a pre-oxidation layer is removed from one side of the sample. Subsequent dual atmosphere exposure at 600 °C for 500 h shows that the pre-oxidation layer on the hydrogen-facing side is more important for corrosion resistance in dual atmosphere than the pre-oxidation layer on the air-facing side.

Introduction

Solid oxide fuel cell (SOFC) technology is a promising future energy conversion system, which could complement or even replace conventional combustion technologies. The SOFC system has many advantages, such as high electrical efficiency, scalability, fuel flexibility, and clean emissions [1,2]. However, some challenges still remain until widespread commercialization can be achieved.

One important component of SOFCs is the interconnect, which connects separate fuel cells in series to form a fuel cell stack with a desired electrical potential [3]. Nowadays, interconnects are typically made of ferritic stainless steels (FSS) and with further advances in other parts of the fuel cell, especially the electrolyte, the lowering of operating temperatures down to 600 °C–850 °C has been made possible [4–6]. However, even though many improvements have been made, such as the switch from ceramic interconnects to ferritic stainless steel interconnects and a decrease in operating

* *Corresponding author.*
E-mail address: goebel@chalmers.se (C. Goebel).
https://doi.org/10.1016/j.ijhydene.2018.05.165

temperatures, interconnects still account for many problems in the SOFC system. One issue, for example, is the material degradation of the interconnectors, which occurs due to corrosion processes that occur during fuel cell operation. Another major problem of the SOFC system is the high cost, which is, to a large part, due to the interconnects [6–8].

Attempts to decrease costs, for example, by using low-cost commercially available steels, such as AISI 441, instead of specifically designed steels, often result in increased corrosion. On the other hand, lower temperatures, around 600 °C–700 °C, are expected to decrease the corrosion of the interconnectors and, thus, allow for the use of cheaper steels. However, depending on exposure conditions and alloy compositions, some studies have not observed decreased corrosion with lower temperatures, but, instead, the opposite has been found, increased corrosion at lower temperatures [9–11]. For example *Young* et al. [11] have stated that ferritic stainless steels in a simulated anode environment exhibited more severe corrosion between 500 and 650 °C than between 650 and 800 °C. *Niewolak* et al. [12] have also observed the formation of breakaway oxidation at 600 °C on ferritic as well as austenitic stainless steels in Ar − 4 %H_2 − 2% H_2O. Therefore, the expectation that lower temperatures will lead to decreased corrosion is an oversimplification, and corrosion behavior in other typical SOFC atmospheres should be reinvestigated at these temperatures.

The effect of the dual atmosphere (air on one side and hydrogen or a different fuel on the other side) present in SOFCs on the corrosion behavior of interconnects was already discussed in the early 2000s and is still being investigated today [13–24]. In some cases, these dual atmosphere conditions led to greater corrosion on the air-facing side than single atmosphere conditions. However, the severity of this so-called dual atmosphere effect has differed between different research groups. Some, such as *Yang* et al. [13], have observed a more drastic effect, and others, such as *Skilbred* et al. [20], have described minor changes in oxide scale composition but no difference in oxide scale thickness. These studies were primarily conducted at temperatures around 800 °C, which warranted us to re-examine the dual atmosphere effect on AISI 441 at 600 °C [21]. We have shown that this material suffers from severe corrosion under dual atmosphere conditions at the lower temperature but that a protective behavior occurs in single atmosphere conditions. This difference is considered evidence that hydrogen somehow affects the air side oxidation process. The breakdown of the protective Cr_2O_3 scale, formed during pre-oxidation, into a non-protective fast growing iron rich oxide scale (i.e. breakaway corrosion) is attributed to the fact that the Cr supply from the metal to the oxide scale is outmatched by the consumption of Cr due to oxide scale growth or other processes such as Cr evaporation. The fact that breakaway corrosion on the air side is only observed under dual atmosphere conditions shows that hydrogen affects either the Cr supply or the Cr consumption. It is however not obvious how hydrogen affects this balance. Mechanisms discussed in the literature include for example doping of the oxide scale, which causes faster growth [13]. For a more detailed discussion on potential mechanisms the reader is referred to *Alnegren* et al. [22]. In this paper it is also shown that the dual atmosphere effect exhibits an inverse temperature-dependency; while a strong dual atmosphere effect was observed at 600 °C, no visible effect was observed at 700 or 800 °C [22]. During these studies, a short pre-oxidation step (180 min) in air before exposure was introduced to simulate the sintering process, which a fuel cell stack is subjected to after assembly. This pre-oxidation step, therefore, resulted in a more accurate representation of the interconnect in a fuel cell.

In the present work, the effect of the pre-oxidation of a ferritic stainless steel interconnect on the corrosion behavior in dual atmosphere is closely examined with regard to two main factors, the pre-oxidation time and the pre-oxidation location (i.e. air side vs. hydrogen side). Both parameters are expected to give more insight into the dual atmosphere effect and could potentially allow for accelerated testing, by varying the pre-oxidation time, and give us the knowledge necessary to design coatings to mitigate the dual atmosphere effect.

Materials and methods

Dual atmosphere setup

All experiments were conducted in dual atmosphere using an experimental setup previously described in *Alnegren* et al. [21]. The sample holder dimensions, design, and construction were based on a model provided by Montana State University, and further information on this setup can be found elsewhere [21,25–27]. The sample holder was custom made, using 253 MA steel. Adapters, welded to the side of the sample holder, connected it to 6 mm 316 L steel tubes. To ensure airtightness, gold rings were used to seal the circular samples to the setup. Regular checks were performed throughout the experiment to see if gas leakage had occurred.

Sample preparation

The influence of pre-oxidation on the dual atmosphere effect was examined with regard to two parameters: pre-oxidation time and pre-oxidation location. Therefore, two different experiments were conducted. AISI 441 was used for all experiments; however, two batches with slightly different compositions (see Table 1) and different thicknesses were used. 0.2 mm thick AISI 441 was used to study pre-oxidation time, while 0.3 mm thick AISI 441 was used to study pre-oxidation location. All samples were manually cut into circles with a diameter of 21 mm and ultrasonically cleaned in acetone and in ethanol. Subsequent pre-oxidation was achieved in humid air (3% H_2O) at 800 °C with a controlled air flow of 280 sml • min^{-1}. To examine the influence of pre-oxidation time on corrosion behavior in dual atmosphere, 5 different pre-oxidation times were chosen: 0, 11, 45, 180, and 280 min. Mass gain data was obtained for the pre-oxidation and, for more accurate data, all pre-oxidations were carried out using duplicate samples.

To study pre-oxidation location, six samples were pre-oxidized for 180 min. The oxide layer was subsequently removed from the hydrogen-facing side, the air-facing side or both sides by grinding (grit #1200), or it was not removed from any side at all. The new sample thickness was roughly 0.2 mm except where no oxide scale was removed. Duplicate

Table 1 – Composition of both AISI 441 batches in weight%.

AISI 441/EN 1.4509	Fe	Cr	Mn	Si	Ti	Nb	Ni	C	S	N
Pre-oxidation time study (0.2 mm thick)	Bal.	17.74	0.30	0.55	0.15	0.37	0.19	0.015	0.002	–
Pre-oxidation location study (0.3 mm thick)	Bal.	17.56	0.35	0.59	0.17	0.39	0.26	0.014	0.001	0.017

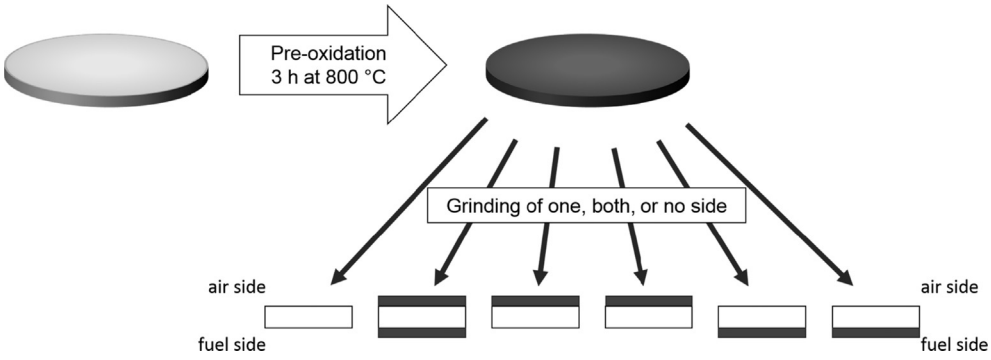

Fig. 1 – Scheme for pre-oxidation location experiment. AISI 441 samples were first pre-oxidized for 3 h at 800 °C in air, and then the oxide layer was removed by grinding (grit #1200).

samples were prepared with a remaining protective oxide layer either on the hydrogen-facing side or on the air-facing side (see Fig. 1).

Exposure

All samples were exposed to a humid dual atmosphere. The following gases were used: Ar – 5% H_2 – 3% H_2O with a flow rate of 100 sml • min^{-1} and air – 3% H_2O with a flow rate of 8800 sml • min^{-1}. This results in flow speeds of around 27 cm • s^{-1} inside the experimental setup and, therefore, kinetically controlled and flow-independent chromium evaporation rates were achieved [28]. To adjust the humidity level to 3%, all gases were bubbled through water baths with temperature controlled reflux condensers attached. All exposures were conducted at a temperature of 600 °C. A ramp of 1 °C • min^{-1} was used for heating up and cooling down purposes. The experiment that investigated the effect of pre-oxidation time was carried out for 1000 h. To visualize the corrosion progress, the exposure was interrupted after 24 h, 168 h, 500 h, and 730 h, and the samples, still mounted in the sample holder, were photographed. The entire run was repeated for 500 h to confirm findings. Only one 500 h isothermal exposure was carried out for the pre-oxidation location experiment, however, duplicate samples were used for the relevant cases (see Fig. 1).

Characterization

After each interruption, pictures were taken of all samples. Detailed analysis using scanning electron microscopy (SEM) was performed after exposure. For top-view images, a FEI Quanta 200 FEG ESEM equipped with an Oxford X-max 80 Energy Dispersive X-ray (EDX) system for chemical analysis was used, while cross-sections were analyzed using a Zeiss LEO Ultra 55 with an Oxford Inca EDX System. Broad Ion Beam (BIB) milling was performed using the Leica EM TIC 3X instrument.

Results and discussion

Pre-oxidation

Mass gain data collected after pre-oxidation of AISI 441 at 800 °C is visualized in Fig. 2. Duplicate samples were pre-oxidized for the study on pre-oxidation time and are marked

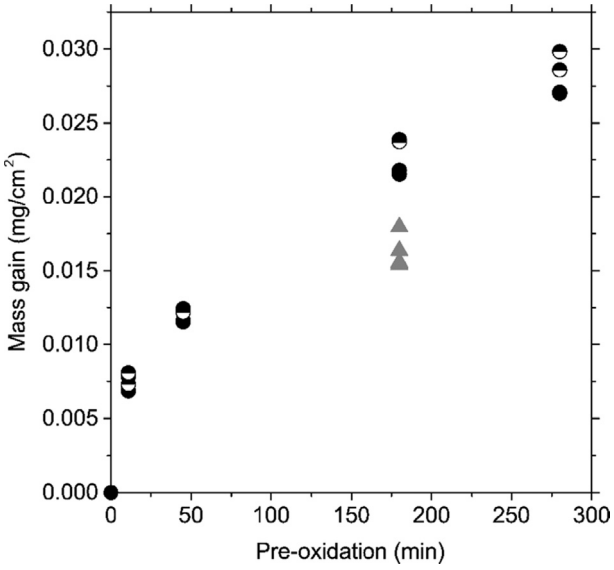

Fig. 2 – Mass gain data on AISI 441 for different pre-oxidation times. Pre-oxidation was carried out at 800 °C in air. Duplicate samples were pre-oxidized for the experiment on pre-oxidation time (circles). Two dual atmosphere exposures were conducted for this study: one 500 h exposure (semi-filled circles) and one 1000 h exposure (filled circles). For the experiment on pre-oxidation location, six samples were pre-oxidized for 180 min (triangles).

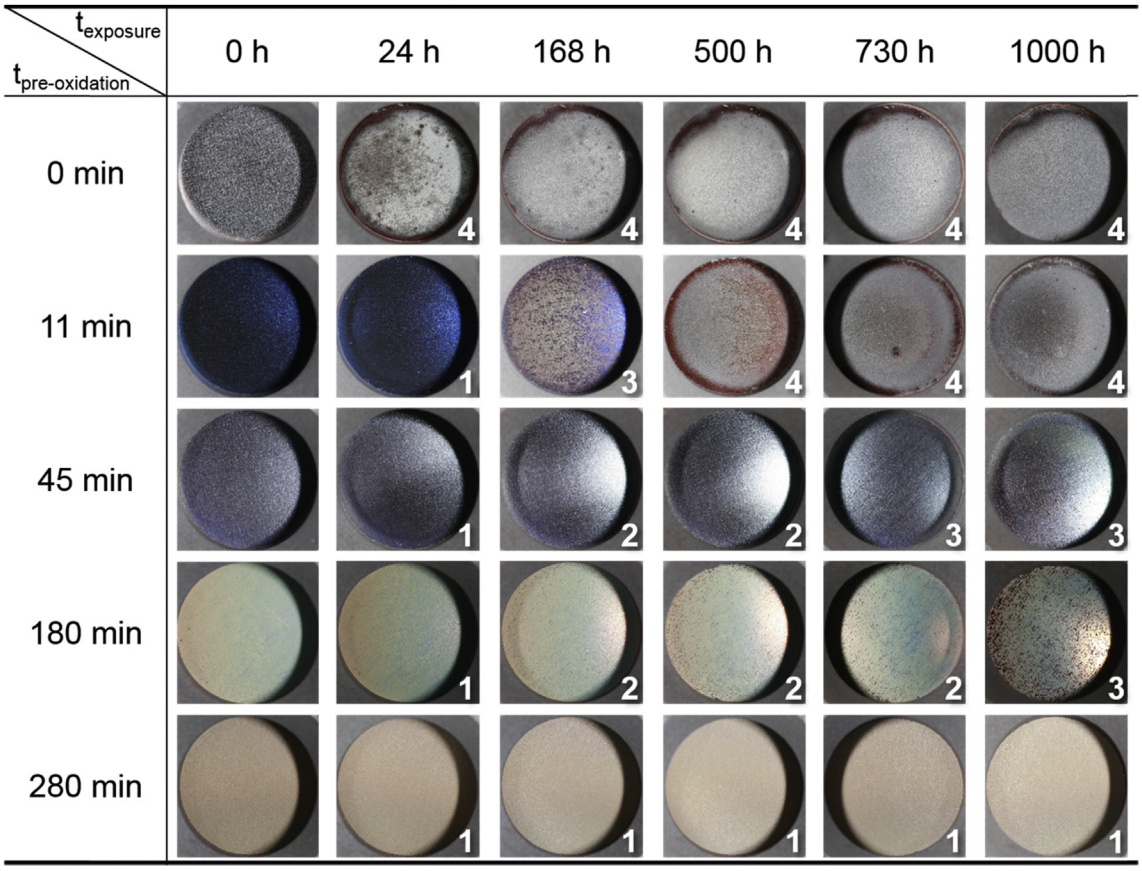

Fig. 3 – Photographs of the air-facing side of AISI 441 taken during discontinuous dual atmosphere exposure at 600 °C. The numbers at the bottom of each picture rate the progress of corrosion, with the following definition for each number: 1 = only protective behavior present, 2 = mostly protective behavior present, 3 = mostly corroded surface, and 4 = completely corroded surface.

as circles. The semi-filled circles represent the samples that were exposed for 500 h, and the filled circles represent samples, that were exposed for 1000 h. The mass gain data shows an approximately parabolic growth for the different pre-oxidation times. Six samples were pre-oxidized for the study on pre-oxidation location, and their mass gains are depicted as triangles in Fig. 2. After 180 min of pre-oxidation the mass gains of the samples used for the pre-oxidation location experiment were slightly lower than the mass gains of the samples used for the experiment on pre-oxidation time. However the mass gains differed only by approximately 0.007 mg cm^{-2} and thus no significant difference in corrosion behavior is expected. This slight deviation is probably due to the fact that two different batches of AISI 441 were used for the experiments. The use of different batches was necessary because a thicker starting material, was needed for the pre-oxidation location experiment, as these samples had to be ground after pre-oxidation.

The general consensus [13,20–22] is that the dual atmosphere only affects the protective oxide layer of the air-facing side and not the one of the hydrogen-facing side. Therefore the focus in the following is on the changes occurring on the oxide layer of the air-facing side. First the results for the experiments on pre-oxidation time and then the results of the experiment on pre-oxidation location are presented and discussed.

Influence of pre-oxidation time on corrosion behavior in dual atmosphere

Visual inspection

Fig. 3 shows photographs that were taken from the air-facing side of all samples during the discontinuous 1000 h dual atmosphere exposure. Similar results were found for the 500 h exposure. Visual inspection clearly showed that the non-pre-oxidized sample experienced breakaway corrosion over the entire surface after 24 h, whereas the rest of the samples showed protective behavior after 24 h. Severe signs of breakaway corrosion were observed on the sample pre-oxidized for 11 min after 168 h of exposure, and this sample was completely covered by breakaway corrosion after 500 h. The sample pre-oxidized for 45 min exhibited few iron-oxide nodules after 168 h, but severe breakaway corrosion was observed after 730 h. This behavior is not clearly apparent in Fig. 3 but was clearly seen at higher magnification. Similar behavior was observed for the sample pre-oxidized for 180 min, and small signs of breakaway corrosion became apparent on this sample after 168 h, but severe breakaway

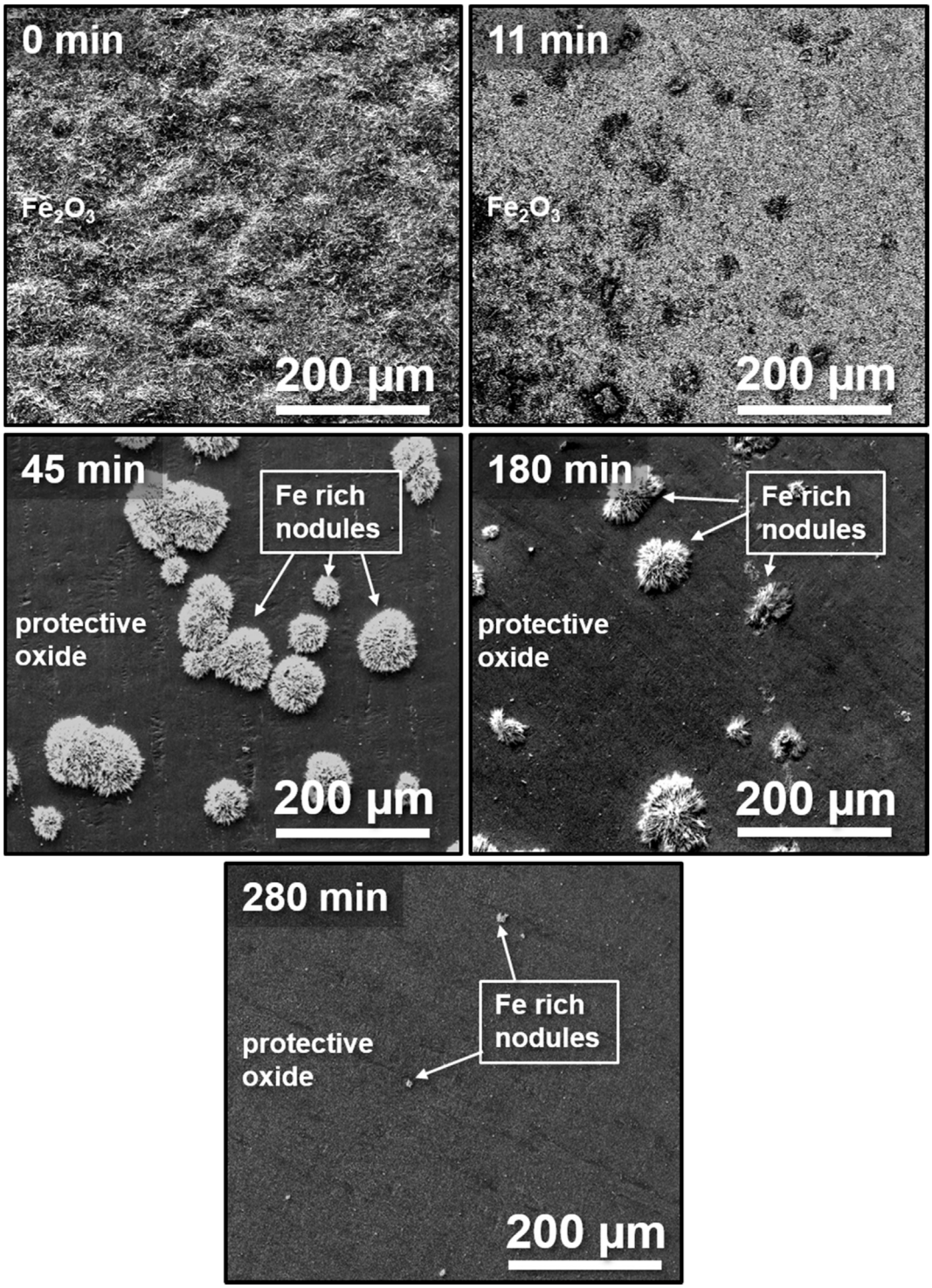

Fig. 4 – SEM micrographs of the air-facing surface of AISI 441 exposed to dual atmosphere for 1000 h at 600 °C. 5 different pre-oxidation times were employed: 0 min, 11 min, 45 min, 180 min, and 280 min.

corrosion only occurred after 1000 h. The sample pre-oxidized for 280 min showed no signs of breakaway corrosion even after 1000 h of exposure in dual atmosphere. These results show a clear correlation between the pre-oxidation times and the onset of breakaway oxidation, which means that longer pre-oxidation times delay the onset of breakaway oxidation under dual atmosphere conditions.

Microstructural analysis

SEM micrographs of the air-facing side of the samples exposed for 1000 h in dual atmosphere are shown Figs. 4 and 5, top-view images and cross-sections, respectively. The compositions were identified with EDX analysis. XRD analysis could not be conducted because all samples were bent after removal from the experimental setup. However, when considering

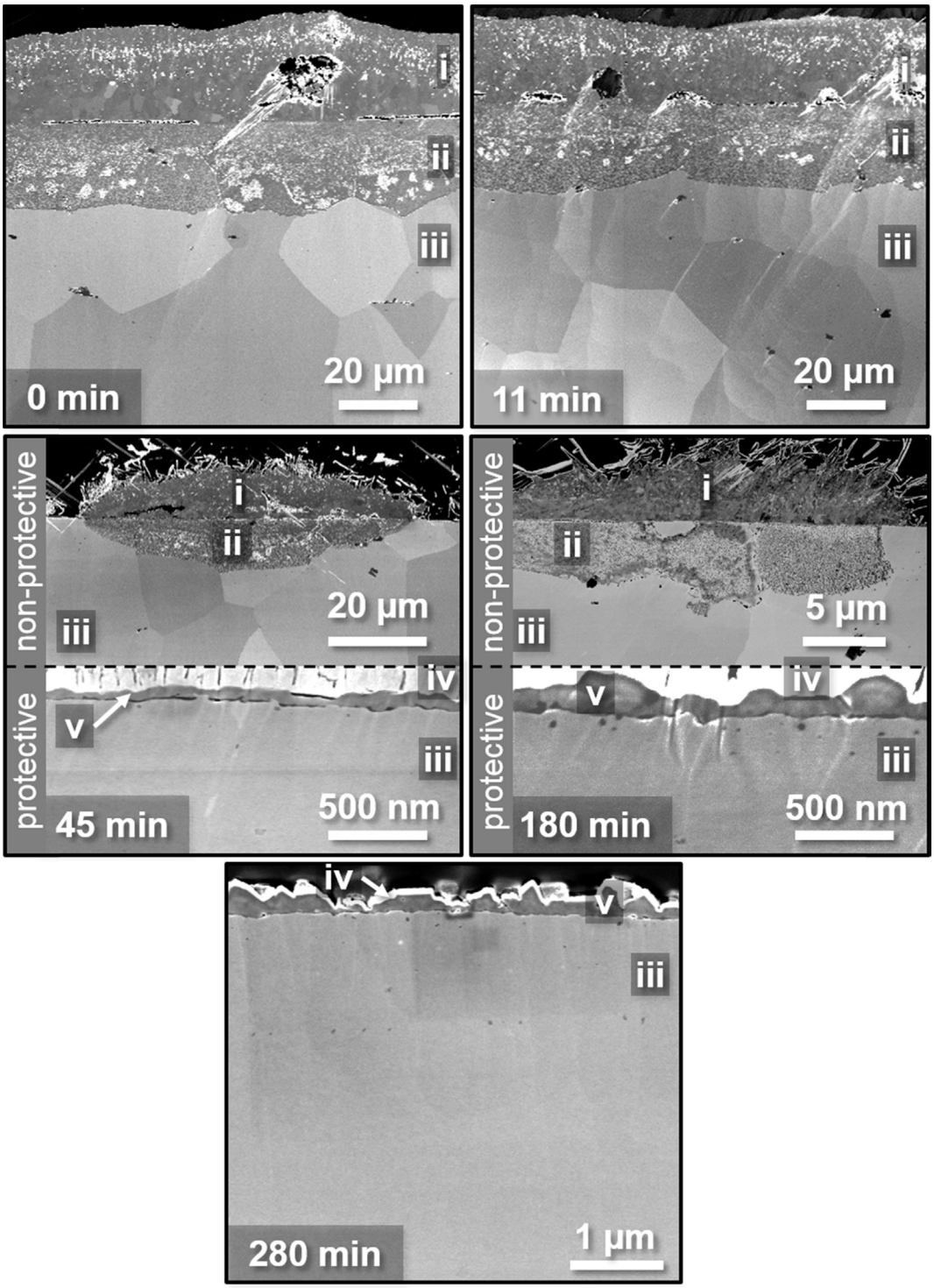

Fig. 5 – SEM micrographs of the air-facing side of AISI 441 cross sections exposed to dual atmosphere for 1000 h at 600 °C. 5 different pre-oxidation times were employed: 0 min, 11 min, 45 min, 180 min, and 280 min. All phases were assigned as follows: i) Fe_2O_3, ii) $(Cr,Fe)_3O_4$, iii) steel, iv) gold coating, v) protective oxide.

experimental studies carried out at 650 °C in air [29] it can be assumed that the remaining protective oxide found on some of the samples consisted of Cr_2O_3 and $(Cr,Mn)_3O_4$. Extensive TEM analyses of AISI 441 pre-oxidized for 180 min and exposed to dual atmosphere at 600 °C for 1000 h can be found in Refs. [21,22].

It is evident in the micrographs in Figs. 4 and 5 that the samples with the shortest pre-oxidation times, namely 0 min and 11 min, suffered severe breakaway corrosion. The entire surfaces of both samples were covered in iron oxide with an atomic weight percent ratio of 2:3 (Fe:O), which is expected to be hematite [30,31]. The cross sections in Fig. 5 reveal a

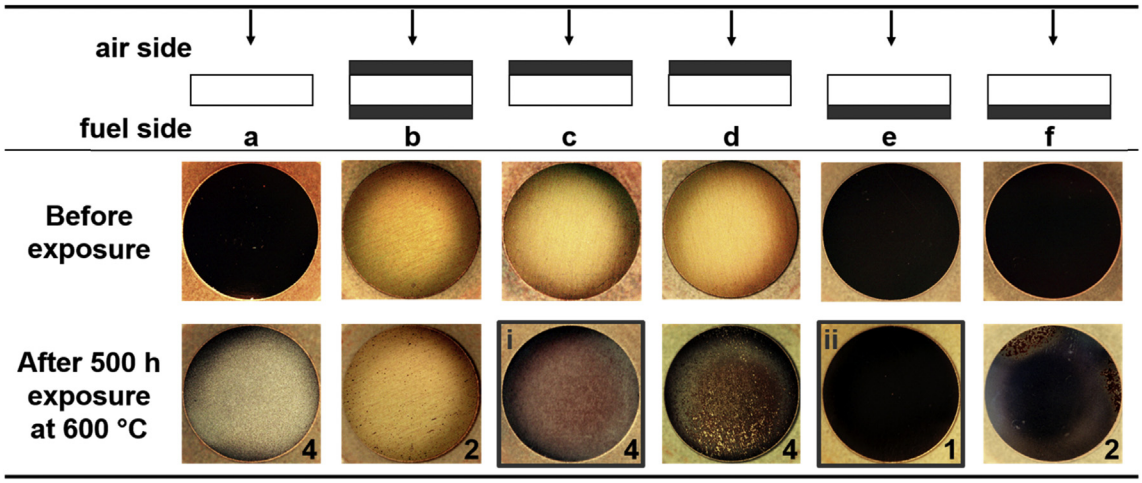

Fig. 6 – Photographs of the air-facing side of AISI 441 exposed to dual atmosphere for 500 h at 600 °C. All samples were pre-oxidized for 180 min in air prior to exposure and, subsequently, one or two or no oxide layers were removed by grinding the sample. The letters a–f identify the different samples as follows: a) pre-oxidation removed from both sides, b) pre-oxidation layer present on both sides, c) and d) pre-oxidation layer removed from the hydrogen-facing side, and e) and f) pre-oxidation layer present on the hydrogen-facing side. The numbers at the bottom of each picture rate the progress of corrosion, with the following definition for each number: 1 = only protective behavior present, 2 = mostly protective behavior present, 3 = mostly corroded surface, and 4 = completely corroded surface. Detailed SEM analysis was performed on the samples marked with i) and ii).

roughly 45 μm thick breakaway oxidation layer for the samples pre-oxidized for 0 min and a roughly 37 μm breakaway oxidation layer for the samples pre-oxidized for 11 min. In both cases, the breakaway layer consisted of an outer hematite and an inner $(Fe,Cr)_3O_4$ layer [30] with similar thicknesses. In contrast, the surfaces of the samples pre-oxidized for 45 min and 180 min were only partially covered with iron rich nodules, and a protective oxide layer was still present on the rest of their surfaces. The morphology of the nodules was, in both cases, similar to the breakaway corrosion layer observed for the non-pre-oxidized and 11 min pre-oxidized samples, with a $(Fe,Cr)_3O_4$ layer present below the hematite layer. The remaining protective oxide layer was roughly 70 nm thick for the sample pre-oxidized for 45 min and 170 nm thick for the sample pre-oxidized for 180 min. The sample pre-oxidized for 280 min performed significantly better in dual atmosphere than all other samples, and very few isolated iron-rich nodules had formed on the surface of that sample. The protective oxide layer found on almost the entire surface was roughly 210 nm thick. SEM images confirmed the conclusion drawn from the visual inspection; there is a correlation between pre-oxidation time and the onset of breakaway corrosion.

The results from the pre-oxidation time experiments clearly showed the importance of pre-oxidation in dual atmosphere. They also confirmed that longer pre-oxidation times lead to an increase in corrosion resistance in dual atmosphere. The opposite is true as well, i.e. shorter pre-oxidation times result in a decrease in corrosion resistance in this atmosphere. Therefore, accelerated testing of different materials might be possible.

Influence of pre-oxidation location on corrosion behavior in dual atmosphere

Visual inspection

Photographs taken from the air-facing side of AISI 441 exposed to dual atmosphere for 500 h at 600 °C are shown in Fig. 6. Visual inspection showed heavy corrosion on the sample where the pre-oxidation layer was removed from both sides (a) and on the samples with the pre-oxidation layer removed from the hydrogen-facing side (c and d). The sample with pre-oxidation layers present on both sides (b) exhibited some signs of breakaway corrosion, whereas hardly any breakaway corrosion was found on the sample with the pre-oxidation layer present on the hydrogen-facing side (e). However, in the latter case, the duplicate sample (f) deviated slightly from sample (e); sample (e) showed no signs of breakaway oxidation on the entire surface, and sample (f) showed breakaway corrosion on the edge of the sample. A closer examination of sample (f) revealed that no breakaway corrosion had occurred in the middle of the sample. This finding, in combination, with the isolated pattern of the breakaway corrosion visible on the sample edge strongly suggests that some hydrogen leakage might have occurred during exposure, and this led to the formation of breakaway corrosion.

Visual inspection clearly showed that the pre-oxidation layer on the hydrogen-facing side is more important for corrosion resistance against the dual atmosphere effect than the pre-oxidation layer on the air-facing side. Another observation was that the sample with a pre-oxidation layer present

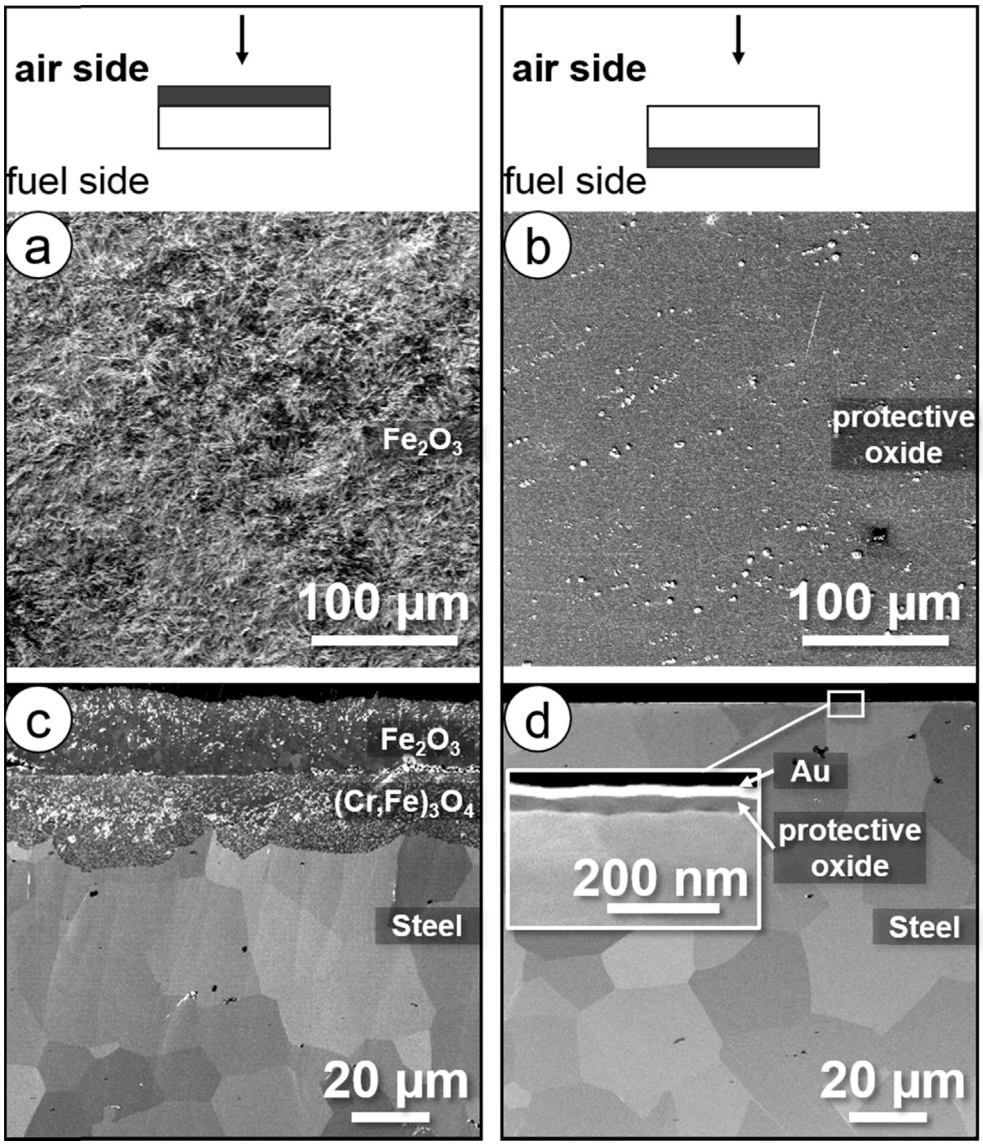

Fig. 7 – SEM micrographs of the air-facing side of AISI 441 exposed to dual atmosphere for 500 h at 600 °C. The samples were pre-oxidized prior to exposure for 180 min in air and, subsequently, the oxide layer on either the air-facing side or the hydrogen-facing side was removed by grinding the sample. A) and c) correspond to the sample where the oxide layer on the hydrogen-facing side was removed, while b) and d) correspond to the sample where the oxide layer on the hydrogen-facing side was present.

on both sides exhibited more breakaway corrosion than the samples with pre-oxidation layers only on the hydrogen-facing side. This is probably due to the different surfaces of the air-facing side of these samples. The sample with a pre-oxidation layer present on both sides received no surface treatment and was exposed to dual atmosphere conditions as-received, whereas the samples with a pre-oxidation layer present only on the hydrogen-facing side were ground on the air-facing side prior to dual atmosphere exposure. The grinding was done to remove the pre-oxidation layer on the air-facing side. Previous studies have found an influence of surface modification on corrosion behavior [12,32,33]. For example, *Niewolak* et al. [12] have seen a beneficial effect of surface grinding and a slightly detrimental effect of surface polishing on corrosion behavior compared to the as-received surface. The general consensus is that by introducing surface defects through the grinding process, Cr diffusion is enhanced, and thus, the formation and upkeep of the protective Cr_2O_3 and $(Cr,Mn)_3O_4$ scales are improved. Therefore, it is not surprising that the samples that were ground on the air-facing side and had a remaining pre-oxidation layer present on the hydrogen-facing side performed slightly better in dual atmosphere than the sample with a pre-oxidation layer on both sides.

Microstructural analysis

A detailed SEM analysis was conducted on the air-facing side of the most relevant samples, the samples with either the pre-oxidation layer present or removed from the hydrogen-facing side. SEM Micrographs of the samples marked with i) and ii) in

Fig. 6 are visualized in Fig. 7. All compositions were confirmed with EDX analysis. The sample with the pre-oxidation layer removed from the hydrogen-facing side showed that Fe_2O_3 covered the entire surface of the sample. This breakaway oxidation layer exhibited a microstructure similar to the one discussed for shorter pre-oxidation times (see section Influence of pre-oxidation time on corrosion behavior in dual atmosphere). Underneath the roughly 20 μm thick Fe_2O_3 layer, an equally thick $(Cr,Fe)_3O_4$ layer had formed. In contrast, the sample with a pre-oxidation layer present on the hydrogen-facing side showed no signs of breakaway oxidation. Instead, a highly protective, roughly 50 nm thick Cr- and Mn-containing oxide layer was observed on the entire sample.

SEM analysis confirmed the results from the visual inspection; the pre-oxidation layer on the hydrogen-facing side is more important for protection against the dual atmosphere effect than the pre-oxidation layer on the air-facing side.

Alnegren et al. [21,22] have discussed the different possible mechanisms for the dual atmosphere effect. The exact mechanism remains unknown and further research is needed, however, the beneficial effect of pre-oxidation in dual atmosphere has been observed [13,21,34]. Two different possible reasons have been proposed for this beneficial effect. The first hypothesis is that the formation of a protective oxide layer on the air-facing side slows down oxidation of the alloy, as a direct air-alloy interface is prevented. The second hypothesis is that the protective oxide layer on the hydrogen-facing side decreases the ingress of hydrogen into the steel and, thus, limits the effect of the dual atmosphere on the corrosion behavior of the air-facing side. The present study clearly proves that the latter hypothesis is more probable. The pre-oxidation layer on the hydrogen-facing side impedes the onset of breakaway corrosion, whereas the pre-oxidation layer on the air-facing side does not. This is also in agreement with previous work by *Kurokawa* et al. [35] on hydrogen permeation through an oxidized FSS at 800 °C. In those studies, it was observed that hydrogen permeation through Cr_2O_3 is substantially slower than diffusion through ferritic stainless steel, and that after 100 h of exposure and the formation of a roughly 760 nm thick Cr_2O_3 scale (on one side), the hydrogen permeation level had decreased by 0.18% [35] compared to hydrogen permeation through the bare alloy. This also suggests that a thicker oxide scale on the hydrogen-facing side enhances the corrosion resistance in dual atmosphere, as less hydrogen dissolution in the alloy occurs. The results observed for different pre-oxidation times in the present study confirm this conclusion. However, these results also strongly suggest that the beneficial effect of the pre-oxidation layer on the hydrogen-facing side might not be sufficiently effective for very long exposure times. It is, therefore, vital to protect the alloy from hydrogen dissolution by other, more effective, means, such as barrier coatings. The results indicate that fuel side coatings might be the most effective.

Conclusion

The present study investigated the influence of the pre-oxidation of uncoated AISI 441 on the dual atmosphere effect. The pre-oxidation time clearly correlated to the onset of breakaway oxidation. This means that under dual atmosphere conditions, longer pre-oxidation times increase corrosion resistance. Consequently, shorter pre-oxidation times should allow for accelerated testing of different materials.

A comparison of samples with the pre-oxidation scale removed from one side showed that the existence of an oxide scale on the hydrogen-facing side was more important to maintaining a protective oxide scale on the air-facing side. The results suggest that a pre-oxidation scale on the hydrogen-facing side acts as a barrier to hydrogen ingress into the steel. The presence of an oxide scale on the air-facing side before dual atmosphere exposure seems to be of less importance. This indicates that barrier coatings on the hydrogen-facing side might be the most efficient in mitigating a dual atmosphere effect.

Acknowledgments

The authors are grateful for funding by the Swedish Energy Agency (grant 2015-009652), the FFI program, as well as the Swedish High Temperature Corrosion Centre.

REFERENCES

[1] Stambouli AB, Traversa E. Solid oxide fuel cells (SOFCs): a review of an environmentally clean and efficient source of energy. Renew Sustain Energy Rev 2002;6:433–55.
[2] Powell M, Meinhardt K, Sprenkle V, Chick L, McVay G. Demonstration of a highly efficient solid oxide fuel cell power system using adiabatic steam reforming and anode gas recirculation. J Power Sources 2012;205:377–84.
[3] Fergus JW. Metallic interconnects for solid oxide fuel cells. Mater Sci Eng A 2005;397:271–83.
[4] Brett DJL, Atkinson A, Brandon NP, Skinner SJ. Intermediate temperature solid oxide fuel cells. Chem Soc Rev 2008;37:1568–78.
[5] Quadakkers WJ, Piron-Abellan J, Shemet V, Singheiser L. Metallic interconnectors for solid oxide fuel cells – a review. Mater High Temp 2003;20:115–27.
[6] Niewolak L, Tietz F, Quadakkers WJ. Interconnects. High-temperature solid oxide fuel cells for the 21st century: fundamentals, design and applications. 2nd ed. 2015. p. 195–254.
[7] Manufacturing cost analysis of 1 kW and 5kW solid oxide fuel cell (SOFC) for auxillary power applications. Battelle; 2014.
[8] Hall TD, McCrabb H, Wu J, Zhang H, Liu X, Taylor J. Electrodeposition of CoMn onto stainless steels interconnects for increased lifetimes in SOFCs. ECS Trans 2011;35:2489–502.
[9] Sánchez L, Hierro MP, Pérez FJ. Effect of chromium content on the oxidation behaviour of ferritic steels for applications in steam atmospheres at high temperatures. Oxid Met 2009;71:173.
[10] Żurek J, Wessel E, Niewolak L, Schmitz F, Kern TU, Singheiser L, et al. Anomalous temperature dependence of oxidation kinetics during steam oxidation of ferritic steels in the temperature range 550–650 °C. Corros Sci 2004;46:2301–17.

[11] Young DJ, Zurek J, Singheiser L, Quadakkers WJ. Temperature dependence of oxide scale formation on high-Cr ferritic steels in Ar–H2–H2O. Corros Sci 2011;53:2131–41.
[12] Niewolak L, Wessel E, Singheiser L, Quadakkers WJ. Potential suitability of ferritic and austenitic steels as interconnect materials for solid oxide fuel cells operating at 600°C. J Power Sources 2010;195:7600–8.
[13] Yang Z, Walker MS, Singh P, Stevenson JW, Norby T. Oxidation behavior of ferritic stainless steels under SOFC interconnect exposure conditions. J Electrochem Soc 2004;151:B669–78.
[14] Kurokawa H, Kawamura K, Maruyama T. Oxidation behavior of Fe–16Cr alloy interconnect for SOFC under hydrogen potential gradient. Solid State Ion 2004;168:13–21.
[15] Ardigo MR, Popa I, Combemale L, Chevalier S, Herbst F, Girardon P. Dual atmosphere study of the K41X stainless steel for interconnect application in high temperature water vapour electrolysis. Int J Hydrogen Energy 2015;40:5305–12.
[16] Yang Z, Xia G-G, Walker MS, Wang C-M, Stevenson JW, Singh P. High temperature oxidation/corrosion behavior of metals and alloys under a hydrogen gradient. Int J Hydrogen Energy 2007;32:3770–7.
[17] Li J, Yan D, Gong Y, Jiang Y, Li J, Pu J, et al. Investigation of anomalous oxidation behavior of SUS430 alloy in solid oxide fuel cell dual atmosphere. J Electrochem Soc 2017;164:C945–51.
[18] Li J, Zhang W, Yang J, Yan D, Pu J, Chi B, et al. Oxidation behavior of metallic interconnect in solid oxide fuel cell stack. J Power Sources 2017;353:195–201.
[19] Yang Z, Xia G, Singh P, Stevenson JW. Effects of water vapor on oxidation behavior of ferritic stainless steels under solid oxide fuel cell interconnect exposure conditions. Solid State Ion 2005;176:1495–503.
[20] Bredvei Skilbred AW, Haugsrud R. The effect of dual atmosphere conditions on the corrosion of Sandvik Sanergy HT. Int J Hydrogen Energy 2012;37:8095–101.
[21] Alnegren P, Sattari M, Svensson J-E, Froitzheim J. Severe dual atmosphere effect at 600 °C for stainless steel 441. J Power Sources 2016;301:170–8.
[22] Alnegren P, Sattari M, Svensson J-E, Froitzheim J. Temperature dependence of corrosion of ferritic stainless steel in dual atmosphere at 600–800 °C. J Power Sources 2018;392:129–38.
[23] Zhao Y, Fergus J. High temperature oxidation behavior of stainless steel 441 in dual atmosphere - effects of flow rate and humidity. ECS Trans 2009;16:57–64.
[24] Huenert D, Schulz W, Kranzmann A. Corrosion behavior of ferritic and martensitic power plant steels under conditions of dual atmospheres. Corrosion 2010;66:126001–7.
[25] Rufner J, Gannon P, White P, Deibert M, Teintze S, Smith R, et al. Oxidation behavior of stainless steel 430 and 441 at 800 °C in single (air/air) and dual atmosphere (air/hydrogen) exposures. Int J Hydrogen Energy 2008;33:1392–8.
[26] Gannon P, Amendola R. High-temperature, dual-atmosphere corrosion of solid-oxide fuel cell interconnects. JOM 2012;64:1470–6.
[27] Holcomb GR, Ziomek-Moroz M, Cramer SD, Covino BS, Bullard SJ. Dual-environment effects on the oxidation of metallic interconnects. J Mater Eng Perform 2006;15:404–9.
[28] Froitzheim J, Ravash H, Larsson E, Johansson LG, Svensson J-E. Investigation of chromium volatilization from FeCr interconnects by a denuder technique. J Electrochem Soc 2010;157:B1295.
[29] Falk-Windisch H, Svensson J-E, Froitzheim J. The effect of temperature on chromium vaporization and oxide scale growth on interconnect steels for Solid Oxide Fuel Cells. J Power Sources 2015;287:25–35.
[30] Liu F, Tang JE, Jonsson T, Canovic S, Segerdahl K, Svensson J-E, et al. Microstructural investigation of protective and non-protective oxides on 11% chromium steel. Oxid Met 2006;66:295–319.
[31] Kofstad P. High temperature corrosion. London and New York: Elsevier Applied Science Publishers Ltd.; 1988.
[32] Bongiorno V, Piccardo P, Anelli S, Spotorno R. Influence of surface finishing on high-temperature oxidation of AISI type 444 ferritic stainless steel used in SOFC stacks. Acta Metall Sin-Engl 2017;30:697–711.
[33] Leistikow S, Wolf I, Grabke HJ. Effects of cold work on the oxidation behavior and carburization resistance of Alloy 800. Mater Corros 1987;38:556–62.
[34] Amendola R, Gannon P, Ellingwood B, Hoyt K, Piccardo P, Genocchio P. Oxidation behavior of coated and preoxidized ferritic steel in single and dual atmosphere exposures at 800°C. Surf Coat Technol 2012;206:2173–80.
[35] Kurokawa H, Oyama Y, Kawamura K, Maruyama T. Hydrogen permeation through Fe-16Cr alloy interconnect in atmosphere simulating SOFC at 1073 K. J Electrochem Soc 2004;151:A1264–8.